

# Molecular dynamics simulations of nanoindentation of $\beta$ -SiC with diamond indenter

A. Noreyan<sup>a</sup>, J.G. Amar<sup>b,\*</sup>, I. Marinescu<sup>a</sup>

<sup>a</sup> Department of MIME, University of Toledo, Toledo, OH 43606, USA

<sup>b</sup> Department of Physics, University of Toledo, Toledo, OH 43606, USA

Received 1 July 2004; received in revised form 24 November 2004; accepted 25 November 2004

## Abstract

We present the results of molecular dynamics simulations of nanoindentation of the Si-terminated (001) surface of cubic silicon carbide ( $\beta$ -SiC) by a diamond tip. In particular, we investigate the dependence of the critical depth and pressure for the elastic-to-plastic transition as a function of indentation velocity, tip size, and workpiece temperature. The nature of the deformation at higher indentation depths is also considered. Our simulations were carried out using the Tersoff SiC potential, which accurately reproduces the lattice and elastic constants of  $\beta$ -SiC. Over the range of indenter sizes used in our simulations, both the critical pressure and the indentation depth decrease with increasing indenter size. Accordingly, the measured hardness is significantly higher than obtained experimentally for larger indenter sizes but decreases with increasing indenter size. In contrast, the critical indentation depth for the elastic-to-plastic transition does not depend on the indenter velocity over the range studied. For indentation depths beyond the critical depth, the pressure increases and saturates at 100 GPa, which corresponds to the experimental pressure at which  $\beta$ -SiC transforms to rocksalt structure. Thus, we conjecture that the observed plastic behavior is related to the onset of a phase transition from the cubic zinc-blende structure to the rocksalt structure under the indenter tip. This is in reasonable agreement with experimental studies of pressure-induced structural transformation in bulk SiC.

© 2004 Elsevier B.V. All rights reserved.

PACS: 62.25+g; 62.20.-x; 60.20.Fe

Keywords: Silicon carbide; Nanoindentation; Phase transitions; Molecular dynamics

## 1. Introduction

Due to its thermal, chemical, and electrical properties, SiC is a good candidate for a variety of applications, including high-temperature electronics, short-wavelength optics, high-power operations, and structural and protective components for use in nuclear fusion reactors [1]. Different polytypes of SiC exist at ambient pressure, which are differentiated by the stacking sequence of the tetrahedrally bonded Si–C bilayers [1]. Among these polytypes,  $\beta$ -SiC (cubic) is of much interest for its electronic properties. In particular, in recent years many theoretical and experimental studies have been carried out to investigate the different properties and possible applications of this material [1–18,29].

The standard processes for machining SiC involve the use of diamond grains as superabrasives [20]. Generally, in grinding, the material removal proceeds through a series of controlled, localized surface fractures, leaving a rough surface, which is unacceptable for most applications [20]. Accordingly, we would like to study in detail the critical depth of cut for ductile machining as well as the dependence of the brittle–ductile transition on processing parameters such as diamond grain-size, temperature of the workpiece, and grinding velocity. In particular, we are interested in understanding the elastic–plastic transition and what accompanies that transition. We note that there have already been a variety of experimental and theoretical studies of nanoindentation in metallic and semiconductor materials [19,22–28]. As a first step towards understanding the grinding process in SiC, here we present the results of molecular dynamics simulations of nanoindentation of

\* Corresponding author. Tel.: +1 419 530 2259; fax: +1 419 530 2723.

E-mail address: jamar@physics.utoledo.edu (J.G. Amar).

the cubic Si-terminated SiC (001) surface by a diamond tip.

## 2. Molecular dynamics simulations

In order to study nanoindentation of SiC by a diamond tip, we have carried out parallel molecular dynamics (MD) simulations using the Tersoff SiC empirical potential [4]. This potential has been successfully used to describe grain boundaries and antiphase boundaries [5] in SiC, to study the native defects and primary damage states and statistics of defect production in displacement cascades [6–8], as well as to investigate the structural, mechanical, thermal vibration and surface properties of  $\beta$ -SiC [9,10].

The Tersoff interatomic potential involves both two- and three-body terms:

$$E = \frac{1}{2} \sum_{i \neq j} V_{ij} \quad \text{where } V_{ij} = f_C(r_{ij})[f_R(r_{ij}) + b_{ij}f_A(r_{ij})] \quad (1)$$

Here  $i$  and  $j$  are labels for the atoms. The term with  $f_R$  represents a repulsive pair potential due to electron overlap, while  $f_A$  represents an attractive pair potential associated with bonding. The function  $f_C$  is merely a smooth cutoff function which limits the range of the potential. The coefficient  $b_{ij}$  (bond order) corresponds to a many-body interaction of the form,

$$b_{ij} = \chi_{ij}(1 + \beta_i^{n_i} \xi_{ij}^{n_i})^{-1/2n_i}, \quad \xi_{ij} = \sum_{k \neq i,j} f_C(r_{ik})g(\theta_{ijk}) \quad (2)$$

where  $g(\theta_{ijk}) = 1 + c_i^2/d_i^2 - c_i^2/[d_i^2 + (h_i - \cos\theta_{ijk})^2]$  and the constants  $\chi_{ij}$ ,  $\beta_i$ ,  $n_i$ ,  $c_i$ ,  $d_i$  and  $h_i$  depend on the atomic species [4] and  $\theta_{ijk}$  is the angle between an  $ij$  bond and an  $ik$  bond. The equations of motion were integrated using the Verlet algorithm [30] with a timestep of 0.175 fs.

In our simulations, the workpiece was taken to have a  $\beta$ -SiC cubic crystal structure (zinc-blende structure) with a lattice constant of 4.32 Å corresponding to the room-temperature lattice constant for  $\beta$ -SiC obtained using the Tersoff potential [4]. The single crystal workpiece was made from a stacking of close-packed layers with a free surface corresponding to the Si-terminated (001) surface. Periodic boundary conditions were assumed in the  $x$ - and  $y$ -directions (parallel to the surface) while the free surface was allowed to relax in the  $z$ -direction.

We note that previous studies have shown that the silicon-terminated  $\beta$ -SiC (001) surface may have different reconstructions depending on the stress level of the surface [31–34]. For example, when the surface is under tensile stress, a  $c(4 \times 2)$  reconstruction is observed [31], while in the case of compressive stress no reconstruction is predicted to occur [32]. In the absence of stress, which is the case considered here, we find that the Tersoff potential leads to a  $p(2 \times 1)$

reconstruction, in good agreement with density-functional theory predictions [32]. However, it should be noted that the predicted energy difference per atom due to the  $p(2 \times 1)$  reconstruction [32] is only a few meV and is thus relatively small compared to the thermal energy at  $T = 300$  K.

In our MD simulations, the workpiece consisted of three types of atoms. The atoms in the bottom two layers were fixed in order to keep the workpiece fixed during indentation. The atoms in the next two layers as well as on the sides of the workpiece were thermostat atoms [35,36] whose temperature is kept fixed in order to dissipate any heat produced by the indentation process. The remaining workpiece atoms underwent constant energy molecular dynamics. In order to speed up the molecular dynamics simulations, which are relatively slow due to the presence of many-body terms, we have developed a parallel code based on atom-decomposition [37]. Our simulations were carried out on the Ohio Supercomputer Center IA32 Beowulf Cluster consisting of 256 1.4 GHz AMD Athlon MP processors. On 28 processors, a system of 34,496 atoms runs at a rate of about 1.5  $\mu$ s/atom/timestep.

In order to investigate the possible dependence of the critical depth and pressure for elastic-to-plastic transformation on workpiece temperature, temperatures ranging from 100 to 450 K were studied. For each temperature the workpiece was first equilibrated for a period of 14 ps, which was much longer than the time needed for the system to reach equilibrium. In all simulations, the indenter was assumed to be rigid. This is a reasonable approximation since diamond is significantly harder than SiC [1]. The diamond indenter was assumed to have a square pyramidal shape with a lattice constant of 3.57 Å, and different tip areas as shown in Table 1. As indicated, six different indenter sizes were considered.

For each indenter size, runs were carried out with different (increasing) workpiece sizes, in order to find the minimum size necessary to avoid finite-size effects during the simulation. In particular, five workpiece sizes were considered: 18,000 atoms ( $64.8 \times \text{Å} \times 64.8 \times \text{Å} \times 43.2 \text{Å}$ ), 25,920 atoms ( $77.8 \times \text{Å} \times 77.8 \times \text{Å} \times 43.2 \text{Å}$ ), 32,000 atoms ( $86.4 \times \text{Å} \times 86.4 \times \text{Å} \times 43.2 \text{Å}$ ), 50,000 atoms ( $108 \times \text{Å} \times 108 \times \text{Å} \times 43.2 \text{Å}$ ) and 67,280 atoms ( $125 \times \text{Å} \times 125 \times \text{Å} \times 43.2 \text{Å}$ ). In all cases, before indenting the indenter was initially held at a distance larger than the cutoff distance from the surface of the workpiece.

In order to study the dependence of the elastic-to-plastic transformation on indentation speed, simulations were carried out with both a ‘slow’ indentation speed (28.5 m/s) and

Table 1  
Parameters describing diamond indenter used in simulations

Number of atoms in indenter	Number of atoms in tip layer	Tip area (Å <sup>2</sup> )	Tip width (Å)
760	13	50.89	7.13
870	25	114.51	10.7
1968	41	205.58	14.26
2496	61	318.08	17.83
3368	85	458	21.4
5530	113	623.4	25.0

a ‘fast’ indentation speed (85.7 m/s). During unloading the indentation velocity was the reverse of that during loading. The total force on the substrate was calculated during indentation, by measuring the change in the total force acting on the indenter atoms. The average applied pressure was also determined by calculating the total force divided by the projected contact area. Since the half-angle of the indenter used in our simulations was 45°, the projected contact area may be estimated using the simple expression,

$$A_{\text{proj}} = (w + 2d)^2 \quad (3)$$

where  $w$  is the tip width, and  $d$  is the indentation depth. We note that in our simulations, the zero of indenter displacement was defined as the point at which the force between the workpiece and the indenter becomes repulsive as the tip approaches the surface.

### 3. Results

Fig. 1 shows the resulting force–displacement curves during loading and unloading as a function of indentation depth for the case of a small indenter (tip width  $w = 7.1 \text{ \AA}$ ) for both slow and fast indentation with a substrate temperature

of 300 K. As can be seen, for this indenter size the force–displacement curve is reversible as long as the indentation depth is less than a critical value  $d_c \simeq 1.95 \pm 0.05 \text{ \AA}$ . However, indentation beyond this value leads to hysteresis, thus indicating the beginning of plastic deformation. We note that the critical depth obtained is essentially the same for both indentation speeds, thus indicating a rather weak dependence of the critical depth on velocity. The negative force observed at positive displacement is due to the attraction of workpiece atoms by the indenter during unloading. Upon unloading this leads to neck formation between the indenter tip and workpiece as has been observed in previous theoretical studies of gold and silicon nanoindentation [21,22].

We have also carried out simulations for significantly larger tip widths up to approximately  $25 \text{ \AA}$  at both fast and slow indentation speeds. As shown in Fig. 2 for a much larger indenter ( $w = 21.4 \text{ \AA}$ ), we again find a very weak dependence on the indentation speed. However, the value of the critical depth for hysteresis ( $d_c \simeq 1.75 \pm 0.05 \text{ \AA}$ ) is somewhat smaller than for the small indenter.

A summary of our results for the case of fast indentation ( $v = 85.7 \text{ m/s}$ ) at  $T = 300 \text{ K}$  is shown in Table 2. As can be seen, the critical depth decreases weakly with increasing tip width. We note that there is a slight deviation from this

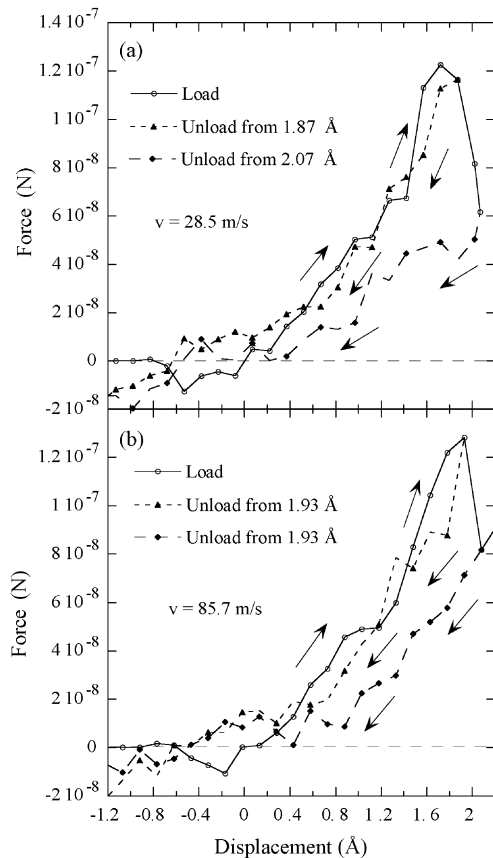


Fig. 1. Force–displacement curve for small indenter (tip width  $7.1 \text{ \AA}$ ) and small workpiece (18,000 atoms,  $64.8 \times \text{ \AA} \times 64.8 \times \text{ \AA} \times 43.2 \text{ \AA}$ ). (a) Slow indentation and (b) fast indentation.

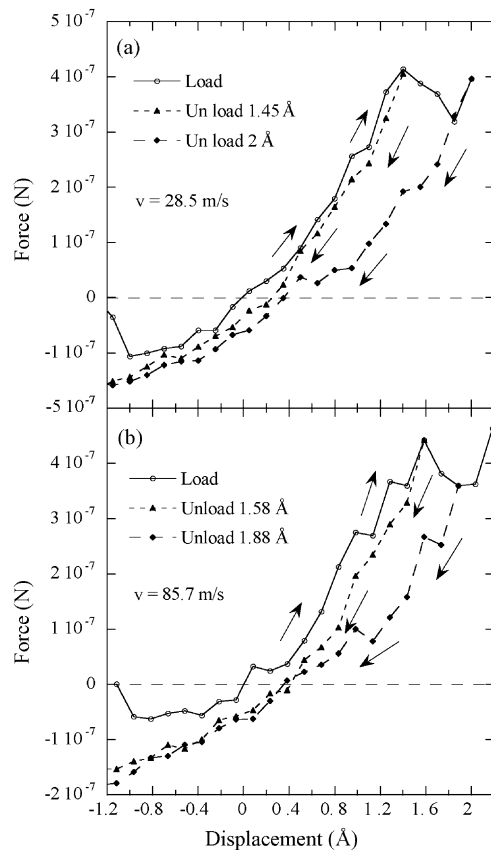


Fig. 2. Force load and unload curves for large indenter (3368 atoms, tip width  $21.4 \text{ \AA}$ ) and large workpiece (50,000 atoms,  $108 \times \text{ \AA} \times 108 \times \text{ \AA} \times 43.2 \text{ \AA}$ ). (a) Slow indentation and (b) fast indentation.

Table 2  
Average critical pressure and critical depth of cut for elastic–plastic transition as function of tip-size for fast indentation at 300 K

Indenter tip width (Å)	Average critical pressure (GPa)	Critical depth (Å)
7.1	107	$1.95 \pm 0.05$
10.7	95	$1.40 \pm 0.05$
14.3	91	$1.80 \pm 0.05$
17.8	93	$1.79 \pm 0.05$
21.4	73	$1.75 \pm 0.05$
25.0	68	$1.55 \pm 0.05$

monotonic behavior for a tip of width  $w = 10.7 \text{ \AA}$ . However, this is most likely due to small differences in the registry between the indenter and the substrate as the indenter tip width is increased. As shown in Table 2, the critical pressure for hysteresis also decreases with increasing indenter tip width.

It is interesting to compare these values with similar results obtained experimentally for larger indenters. Typically, the hardness  $H$  is defined as equal to the peak force applied during indentation divided by the projected contact area [40]. We note that the calculated hardness  $H \simeq 68 \text{ GPa}$  for our largest (2.5 nm) indenter is approximately twice as large as the value  $H \simeq 35 \text{ GPa}$  obtained experimentally by Page et al. [39] using a 100 nm indenter. However, since our measured values for the critical pressure decrease with increasing indenter size, we expect that a simulation of a larger indenter would lead to better agreement with this experiment. We also note that the existence of defects may also play an important role in controlling the hardness for large indenter size.

We have also investigated the dependence of the critical depth for hysteresis on the workpiece temperature by carrying out simulations for five different temperatures in the range from 100 to 450 K. While the critical depth was observed to decrease slightly with increasing temperature, the weakness of this effect suggests that it may in fact be due primarily to thermal expansion [9,10,38]. Since in our simulations, we assumed a fixed system size corresponding to the room-temperature lattice constant of  $\beta$ -SiC. We therefore conclude that there is at most a very weak dependence of the critical indentation depth on both substrate temperature and indentation velocity.

We note that at the critical depth the deformation already extends below the first few layers. However, at this depth the main deformation corresponds to the breaking of bonds in the top two layers around the edge of the indenter. In order to further understand the nature of the plastic deformation, we have also carried simulations with a deeper indentation depth. As can be seen in Fig. 3, for the case of a large indenter, the hysteresis increases with increasing indentation depth, while the average pressure also increases. However, beyond an indentation depth of approximately 5–6 Å the pressure saturates at a value of approximately 100 GPa.

We now consider the nature of the elastic-to-plastic transition observed in our simulations. While plastic deformation was observed for indentations beyond the critical depth, no clear evidence of dislocations was found. This is perhaps

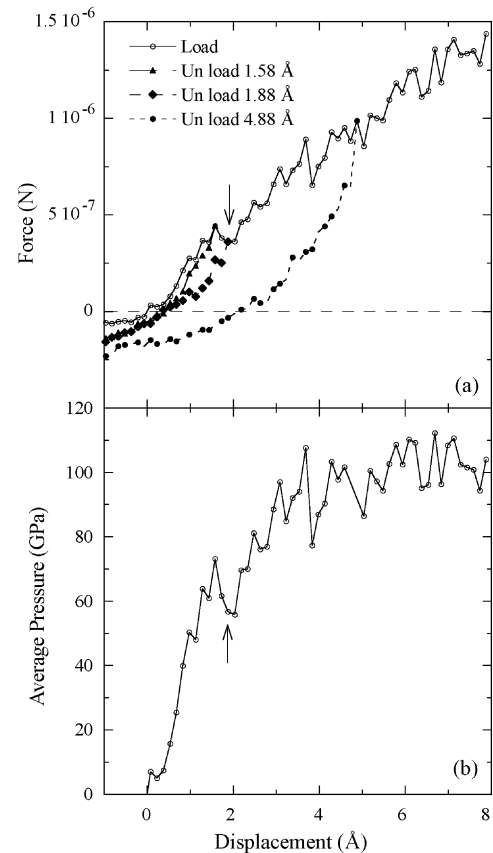


Fig. 3. (a) Force–displacement curve for large indenter (3368 atoms, tip width 21.4 Å) and large workpiece for indentation beyond the critical depth. (b) Corresponding applied pressure as function of indentation depth. Arrows correspond to critical indentation depth.

not surprising given the relatively small indentation depth. We note that in X-ray diffraction studies, Yoshida et al. [2] have reported a pressure-induced phase transition in  $\beta$ -SiC at 100 GPa from the zinc-blende to the rocksalt structure. They also observed a big hysteresis in the pressure load–unload curve due to these transformations [2]. Since the saturation pressure observed in our simulations is very close to that observed experimentally for the pressure-induced phase transition in  $\beta$ -SiC, this suggests that the deformation observed in our simulations at large indentation depth may be related to this pressure-induced phase transformation. In this connection, we note that in recent simulations of nanoindentation of Si [25,27] a phase transformation has also been observed.

In order to test for the occurrence of a phase transformation in our simulations, we have measured the pair-correlation function in a rectangular region of size  $28 \text{ \AA} \times 28 \text{ \AA} \times 8 \text{ \AA}$  surrounding the tip of the indenter both before indentation as well as after indenting beyond the critical depth (arrows in Fig. 3a and b). We note that the lattice constant of  $\beta$ -SiC obtained using the Tersoff potential is in good agreement with the experimental value ( $a = 4.36 \text{ \AA}$ ). Therefore, as shown in Fig. 4, before indentation we obtain pair-correlation function peaks at 1.87 and 3.055 Å as expected, corresponding to the nearest-neighbor and next-nearest-neighbor distances, re-

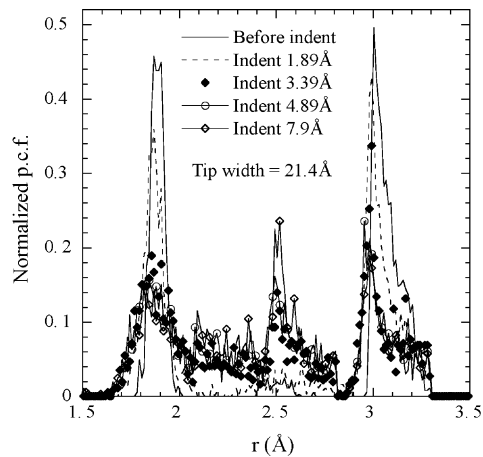


Fig. 4. Pair correlation plots before and after indentation.

spectively. In contrast, for the experimentally observed rocksalt SiC structure ( $a = 3.68 \text{ \AA}$ ), first, second, and third neighbor peaks are expected at 1.84, 2.60, and 3.18  $\text{\AA}$ , respectively.

As can be seen in Fig. 4, after indentation to a depth of 4.9  $\text{\AA}$  or higher, the first-neighbor peak is significantly reduced and widened while its location (1.85  $\text{\AA}$ ) is slightly shifted to the left, in rough agreement with the expected first neighbor peak for the rocksalt structure. A broad peak at approximately 2.5  $\text{\AA}$  is also indicated, again in rough agreement with the expected second-neighbor peak at 2.6  $\text{\AA}$  for the rocksalt structure. Finally, while the amplitude of the third-neighbor peak is reduced, its location (3.0  $\text{\AA}$ ) is also close to that expected for the rock salt structure. Thus, these changes are consistent with a phase transition to the rocksalt structure, although the expected sharp peaks are not fully reproduced.

We have also studied the bond-angle distribution as a function of indentation depth in order to further understand the structural changes due to indentation. In order to study the bond-angle distribution, we assigned a bond between any pair of workpiece atoms whose distance is less than 2.2  $\text{\AA}$ , since this distance is larger than the nearest-neighbor distances for the zinc-blende and rocksalt structures but significantly smaller than the second neighbor distance. We note that in the cubic  $\beta$ -SiC zinc-blende structure the angle between nearest-neighbor bonds is  $109.5^\circ$ , while the bond angle is  $90^\circ$  in the rocksalt structure. As can be seen in Fig. 5, after indentation the dominant peak at  $109^\circ$  remains although it is weakened and significantly broadened. At the same time, however, two new broad peaks appear which are centered at approximately  $56$  and  $77^\circ$ . While these values are somewhat different from the expected peak values ( $45$  and  $90^\circ$ ) for the rocksalt structure, they are suggestive of a transition to a structure which has some similarities to the rocksalt structure.

We may interpret these results as follows. While the Tersoff potential may accurately describe the covalently bonded  $\beta$ -SiC and 6H structures, it does not properly take into account ionic bonding and so cannot accurately reproduce the rocksalt structure, as indicated by the fact that the lattice constant of the Tersoff rocksalt SiC structure [4] is somewhat

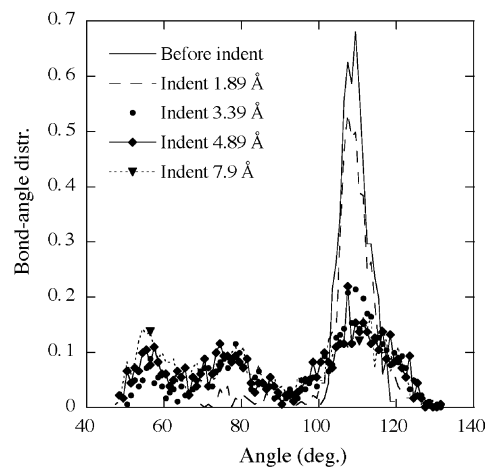


Fig. 5. Bond-angle distribution function before and after indentation.

larger than the experimental value. Accordingly, we expect that while our simulations may accurately describe the onset of a phase transition due to indentation they cannot describe the full transition to the rocksalt structure. This interpretation is supported by the fact that in our simulations the pressure saturates at a value (approximately 100 GPa) which is in good agreement with that observed experimentally for the phase transition from  $\beta$ -SiC to the rocksalt structure [2].

#### 4. Conclusion

Using molecular dynamics we have studied the dependence of the elastic–plastic transition during nanoindentation of  $\beta$ -SiC by diamond, on indenter velocity, size, and workpiece temperature. We found that for indentation velocities ranging from 28.5 to 85.7 m/s, the critical depth for the elastic-to-plastic transformation of  $\beta$ -SiC during indentation depends only weakly on the indentation velocity. In addition, we found that there is at most a very weak dependence of the critical depth on workpiece temperature over the temperature range 100–450 K.

We have also studied the dependence of the critical pressure for the elastic-to-plastic transition on indenter size. In particular, we found that the critical pressure decreases with increasing tip width. Similarly, we found that the critical depth decreases weakly and roughly monotonically with increasing indenter tip width. We note that the critical depth obtained in our simulations (1.4–2.0  $\text{\AA}$ ) is less than twice the layer spacing for  $\beta$ -SiC and corresponds essentially to breaking the first two planes. This value is approximately three times smaller than that found in simulations of nanoindentation in metals [23,24] which is consistent with the fact that SiC is much harder than a typical metal.

We have also studied the nature of the deformation corresponding to indentation beyond the critical depth. In particular, we found that with increasing indentation depth, the pressure increases and then saturates at 100 GPa, which

corresponds to the experimental pressure at which a phase transformation from the zinc-blende to rocksalt structure occurs. As already noted, we believe that this indicates the onset of a phase-transformation from the  $\beta$ -SiC structure to the rocksalt structure. Such an interpretation is supported by our results for the pair-correlation function and bond-angle distribution after indentation, which suggest a transition to a structure which is similar to the SiC rocksalt structure. This is consistent with the fact that while the Tersoff potential describes the covalently bonded  $\beta$ -SiC and 6H structures accurately, it does not properly take into account ionic bonding and so cannot accurately reproduce the rocksalt structure. Thus, we expect that even though the full transition to a rocksalt structure is not properly reproduced, our simulations accurately predict the onset of a phase transition during indentation.

### Acknowledgments

We would like to acknowledge support from the Petroleum Research Fund of the American Chemical Society and from the NSF through grant no. DMR-0219328. We would also like to thank the Ohio Supercomputer Center for a grant of computer time.

### References

- [1] H. Markoc, S. Strite, G. Gao, M. Lin, B. Sverdlov, M. Burns, *J. Appl. Phys.* 76 (1994) 1363.
- [2] M. Yoshida, A. Onodera, M. Ueno, K. Takemura, O. Shimomura, *Phys. Rev. B* 48 (1993) 10587.
- [3] F. Shimojo, I. Ebbsjo, R.K. Kalia, A. Nakano, J.P. Rino, P. Vashishta, *Phys. Rev. Lett.* 84 (2000) 3338.
- [4] J. Tersoff, *Phys. Rev. B* 39 (1989) 5566.
- [5] C. Kohler, *Phys. Stat. Sol. (b)* 234 (2002) 522.
- [6] L. Malerba, J.M. Perlado, *Phys. Rev. B* 65 (2002) 045202.
- [7] R. Devanathan, W. Weber, F. Gao, *J. Appl. Phys.* 90 (2001) 2303.
- [8] F. Gao, E. Bylaska, W. Weber, L. Corrales, *Nucl. Inst. Methods B* 180 (2001) 286.
- [9] M. Tang, S. Yip, *Phys. Rev. B* 52 (1995) 15150.
- [10] L. Porter, J. Li, S. Yip, *J. Nucl. Mat.* 246 (1997) 53.
- [11] H. Yan, A.P. Smith, H. Jonsson, *Surf. Sci.* 330 (1995) 265.
- [12] K. Karch, P. Pavone, W. Windl, O. Schutt, D. Strauch, *Phys. Rev. B* 50 (1994) 17054.
- [13] F. Gao, W.J. Weber, *Nucl. Inst. Meth. B* 191 (2002) 504.
- [14] K. Karch, F. Bechstedt, P. Pavone, D. Strauch, *Phys. Rev. B* 53 (1996) 13400.
- [15] K. Karch, P. Pavone, A.P. Mayer, F. Bechstedt, D. Strauch, *Physica B* 219/220 (1996) 448.
- [16] G. Galli, L. Pizzagalli, A. Catellani, F. Gygi, A. Baratoff, *Appl. Surf. Sci.* 162/163 (2000) 1.
- [17] M.S. Miao, M. Prikhodko, W.R.L. Lambrecht, *Phys. Rev. B* 66 (2002) 064107.
- [18] M. Prikhodko, M.S. Miao, W.R.L. Lambrecht, *Phys. Rev. B* 66 (2002) 125201.
- [19] G.S. Smith, E.B. Tadmor, E. Kaxiras, *Phys. Rev. Lett.* 84 (2000) 1260.
- [20] I. Marinescu, H. Tonshoff, I. Inasaki, *Handbook of Ceramic Grinding and Polishing*, William Andrews Publishing, Noyes, 2000.
- [21] M.R. Sorensen, K.W. Jacobsen, H. Jonsson, *Phys. Rev. Lett.* 77 (1996) 5067.
- [22] R. Astala, M. Kaukonen, R.M. Nieminen, T. Heine, *Phys. Rev. B* 61 (2000) 2973.
- [23] Y. Leng, G. Yang, Y. Hu, L. Zheng, *J. Mat. Sci.* 35 (2000) 2061.
- [24] J. Knap, M. Ortiz, *Phys. Rev. Lett.* 90 (2003) 226102-1.
- [25] W.C.D. Cheong, L.C. Zhang, *Nanotechnology* 11 (2000) 173.
- [26] P. Walsh, A. Omeltchenko, R.K. Kalia, A. Nakano, P. Vashishta, *Appl. Phys. Lett.* 82 (2003) 118.
- [27] C.F. Sanz-Navarro, S.D. Kenny, R. Smith, *Nanotechnology* 15 (2004) 692.
- [28] V. Domnich, Y. Gogotsi, *Rev. Adv. Mater. Sci.* 3 (2002) 1.
- [29] K. Jarrendahl, R.F. Davis, in: *Semiconductors and Semimetals*, vol. 52, Academic Press, New York, 1966.
- [30] M. Allen, D. Tildesley, *Computer Simulation of Liquids*, Oxford University Press, New York, 2001.
- [31] P. Soukiassian, F. Semond, L. Douillard, A. Mayne, G. Dujardin, L. Pizzagalli, C. Joachim, *Phys. Rev. Lett.* 78 (1997) 907.
- [32] A. Catellani, L. Pizzagalli, G. Galli, *Mater. Sci. Eng. B* 96 (2002) 132.
- [33] L. Pizzagalli, C. Joachim, A. Mayne, G. Dujardin, F. Semond, L. Douillard, P. Soukiassian, *Thin Solid Films* 318 (1998) 136.
- [34] P. Soukiassian, *Mater. Sci. Eng. B* 96 (2002) 115.
- [35] S. Nose, *J. Chem. Phys.* 81 (1984) 511.
- [36] J. Jacobsen, B.H. Cooper, J.P. Sethna, *Phys. Rev. B* 58 (1998) 15847.
- [37] S. Plimpton, *J. Comp. Physics* 117 (1995) 1.
- [38] D. Talwar, J. Sherbondy, *Appl. Phys. Lett.* 67 (1995) 3301.
- [39] T.F. Page, G.M. Pharr, J.C. Hay, et al., *Mat. Res. Soc. Symp. Proc.* 522 (1998) 53.
- [40] W.C. Oliver, G.M. Pharr, *J. Mater. Res.* 7 (1992) 1564.